

DETECTION OF PHOSPHORUS, SULPHUR, AND ZINC IN THE
CARBON-ENHANCED METAL-POOR STAR BD+44°493[†]IAN U. ROEDERER,^{1,2} VINICIUS M. PLACCO,^{2,3} AND TIMOTHY C. BEERS^{2,3}*Accepted for publication in the Astrophysical Journal Letters*

ABSTRACT

The carbon-enhanced metal-poor star BD+44°493 ([Fe/H] = −3.9) has been proposed as a candidate second-generation star enriched by metals from a single Pop III star. We report the first detections of P and S and the second detection of Zn in any extremely metal-poor carbon-enhanced star, using new spectra of BD+44°493 collected by the Cosmic Origins Spectrograph on the *Hubble Space Telescope*. We derive [P/Fe] = −0.34 ± 0.21, [S/Fe] = +0.07 ± 0.41, and [Zn/Fe] = −0.10 ± 0.24. We increase by ten-fold the number of Si I lines detected in BD+44°493, yielding [Si/Fe] = +0.15 ± 0.22. The [S/Fe] and [Zn/Fe] ratios exclude the hypothesis that the abundance pattern in BD+44°493 results from depletion of refractory elements onto dust grains. Comparison with zero-metallicity supernova models suggests that the stellar progenitor that enriched BD+44°493 was massive and ejected much less than 0.07 M_{\odot} of ⁵⁶Ni, characteristic of a faint supernova.

Subject headings: nuclear reactions, nucleosynthesis, abundances — stars: abundances — stars: individual (BD+44 493)

1. INTRODUCTION

Carbon-enhanced metal-poor stars with no enhancements of n -capture elements (CEMP-no; Beers & Christlieb 2005) may have formed from the yields of only a single prior generation of zero-metallicity Pop III stars, and perhaps only one star. Norris et al. (2013) summarize this evidence for this hypothesis, linking carbon enhancement and low metallicity with remote, chemically-primitive regions that experienced few enrichment events (e.g., Frebel et al. 2010; Cooke et al. 2011; Carollo et al. 2012). Comparing model yields to the detailed abundance patterns observed in CEMP-no stars provides a rare opportunity to constrain the nature and mechanics of low- or zero-metallicity supernovae (SNe). Stars that produce high C/Fe ratios in the early Universe may include massive, rapidly-rotating, zero-metallicity stars (Meynet et al. 2006) and SNe or hypernovae that experienced mixing and fallback explosions (e.g., Umeda & Nomoto 2003; Ishigaki et al. 2014).

There are approximately 70 confirmed members of the class of CEMP-no stars (Placco et al. 2014b), but only one, BD+44°493, is sufficiently bright ($V = 9.1$) to readily observe in the ultraviolet (UV) with the echelle spectrographs on the *Hubble Space Telescope* (*HST*). BD+44°493 is a red giant located ~ 200 pc from the Sun on a typical halo orbit (Ito et al. 2013). It shows no evidence of stellar companions, as radial velocity measurements constant to within ≈ 0.6 km s^{−1}

span more than 31 years (Carney et al. 2003; Hansen et al. 2016, and references therein). BD+44°493 is extremely metal-poor ([Fe/H] = −3.88 ± 0.19), carbon-enhanced ([C/Fe] = +1.23 ± 0.20), and exhibits low levels of elements produced by n -capture reactions (e.g., [Ba/Fe] = −0.60 ± 0.12). This fortuitous combination of characteristics was first identified by Ito et al. (2009). Ito et al. (2013) performed a detailed abundance analysis of BD+44°493 using high-quality optical spectra. Takeda & Takada-Hidai (2013), Placco et al. (2014a), Roederer et al. (2014a), and Aoki (2015) confirmed the C-enhanced nature of BD+44°493. Placco et al. (2014a) presented the first abundance analysis of the UV spectrum (2280–3100 Å) of BD+44°493, which included several elements not detectable in optical spectra.

Here, we report the detection of phosphorus (P, $Z = 15$), sulphur (S, $Z = 16$), and zinc (Zn, $Z = 30$) in BD+44°493. These are the first detections of P and S and the second detection of Zn in any CEMP-no star with [Fe/H] $\lesssim -4$. Expanding the inventory of elements for even a single member of the class of CEMP-no stars provides critical insight into at least one of the likely progenitors of such stars in the early Universe.

2. OBSERVATIONS

We have obtained new observations of portions of the UV spectrum of BD+44°493 using the Cosmic Origins Spectrograph (COS; Green et al. 2012) on *HST*. Three medium-resolution grating settings were used to collect spectra covering ~ 270 Å between 1799 and 2348 Å in nine non-contiguous stripes of ~ 30 Å each. The spectral resolving power, measured from the PtNe comparison lamp spectra, ranges over $13,000 < R < 17,000$. Table 1 presents a log of these observations, including the date, exposure time (t_{exp}), grating setting, central wavelength setting (λ_c), wavelengths observed (λ), and signal-to-noise ratios (S/N) per pixel after all observations have been co-added.

3. ANALYSIS

[†] Based on observations made with the NASA/ESA *Hubble Space Telescope*, obtained at the Space Telescope Science Institute (STScI), which is operated by the Association of Universities for Research in Astronomy, Inc. (AURA) under NASA contract NAS 5-26555. These observations are associated with program GO-14231.

¹ Department of Astronomy, University of Michigan, 1085 S. University Ave., Ann Arbor, MI 48109, USA; iur@umich.edu

² Joint Institute for Nuclear Astrophysics and Center for the Evolution of the Elements (JINA-CEE), USA

³ Department of Physics, University of Notre Dame, Notre Dame, IN 46556, USA

Table 1
Log of Observations

Date	t_{exp} (s)	Grating	λ_c (Å)	λ^a (Å)	S/N
2015 Nov 21	8417	G225M	2233	2120–2153	20
				2222–2249	40
				2320–2348	55
2015 Nov 22	8301	G185M	1971	1855–1886	12
				1957–1987	20
				2060–2090	30
2015 Dec 04,08,09	31035	G185M	1913	1799–1829	10
				1902–1932	35
				2006–2034	55

Note. — All observations are associated with datasets LCTQ01010–06010 in the Mikulski Archive for Space Telescopes (MAST).

^a Air wavelengths are given for $\lambda > 2000$ Å and vacuum values below. Values given are corrected to rest wavelengths.

We adopt the model atmosphere parameters for BD+44°493 derived by Ito et al. (2013): T_{eff} , 5430 ± 150 K; $\log g$, 3.4 ± 0.3 ; microturbulence velocity, 1.3 ± 0.3 km s^{−1}; and [M/H], -3.8 ± 0.2 . We use a 1D plane-parallel model interpolated from the ATLAS9 α -enhanced grid of Castelli & Kurucz (2003), and we derive abundances using a recent version of the spectrum analysis code MOOG (Snedden 1973; Sobeck et al. 2011).

Figure 1 shows sections of the COS spectra of BD+44°493. Note that the continuum is visible and the lines of interest are unblended. We measure equivalent widths (EW) by fitting the observed lines with a convolution of a Gaussian and the COS line spread function (LSF; Ghavamian et al. 2009). Part of our COS spectrum overlaps (2320–2348 Å) with the Space Telescope Imaging Spectrograph (STIS) spectrum analyzed by Placco et al. (2014a), and we compare EWs in this region to check our measurements. Failure to account for the COS LSF, which redistributes absorption from the line core to the wings, leads to an underestimate of the EWs by $\sim 25\%$. When the COS LSF is included, the EWs measured from the COS and STIS spectra agree to better than 5%. We regard the standard deviation of the residuals, 6.8 mÅ, as the minimum uncertainty in our EWs.

4. RESULTS

The EWs, atomic data, and abundances derived for each line are listed in Table 2. Table 3 lists the mean abundances. We calculate uncertainties as described in Roederer et al. (2014b). We adopt the Solar reference abundances given in Asplund et al. (2009).

Table 3 compares our abundances with those derived by previous studies. Our Fe abundances are in agreement with those derived from other optical and UV lines, indicating that there are no significant zero-point differences. The [Mg/Fe], [Ti/Fe], [Co/Fe], and [Ni/Fe] ratios are also in agreement with previous work. The [Cr/Fe] we derive from Cr II lines agrees with the Placco et al. (2014a) value, but it is higher than the Ito et al. (2013) value. If we adopt the $\log gf$ scale from Nilsson et al. (2006), whose $\log gf$ values for the two Cr II lines examined by us agree to within 0.02 dex with the Bergeson & Lawler (1993) $\log gf$ values, the Ito et al. [Cr II/Fe] ratio would increase by ≈ 0.2 dex. This resolves the discrepancy.

We have detected several Co II lines, which may be

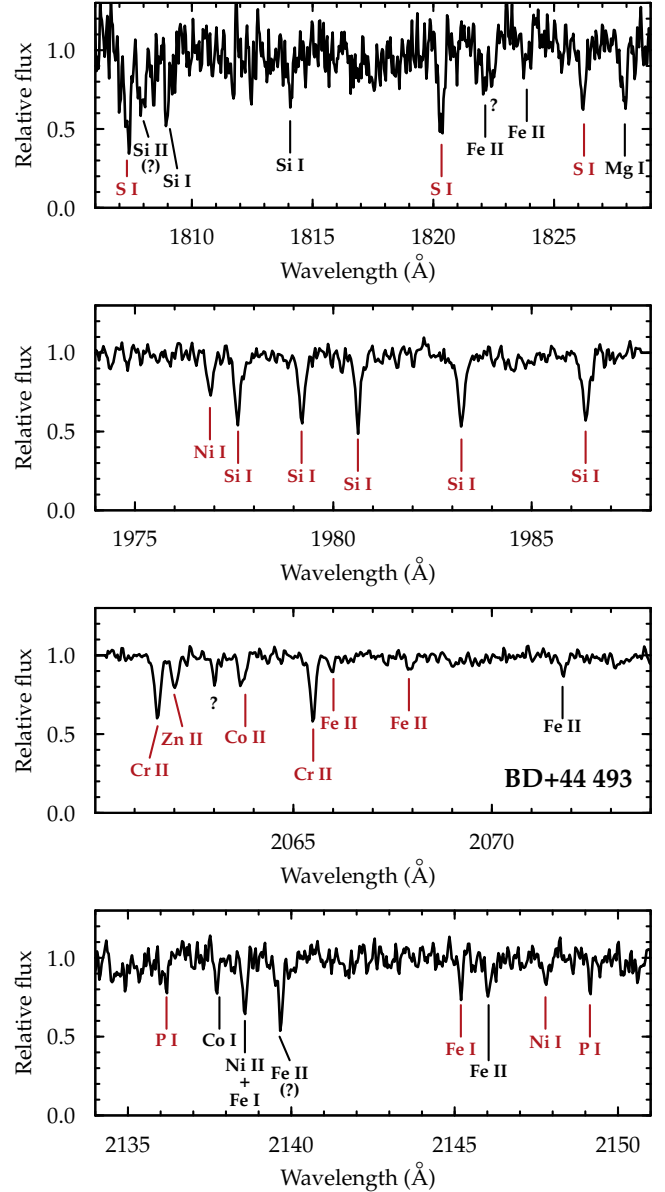


Figure 1. Sections of the COS spectra of BD+44°493. Lines that have been used to derive abundances are marked in red. Uncertain or unknown line identifications are labeled with a question mark; these lines are not used and do not adversely affect our analysis.

Table 2
Atomic Data, Equivalent Widths, and Abundances Derived from Individual Lines

Spec.	λ^a (Å)	E.P. (eV)	$\log gf$	Ref.	EW (mÅ)	$\log \epsilon$
Mg I	2025.82	0.00	−0.95 (0.03)	1	208.4	4.23 (0.50)
Si I	1874.84	0.78	−0.77 (0.30)	1	107.7	4.05 (0.46)

References. — 1: NIST; 2: Bergeson & Lawler (1993); 3: Wood et al. (2014); 4: Fedchak & Lawler (1999); 5: Roederer & Lawler (2012)

Note. — The complete version of Table 2 is available in the online edition of the Journal. A short version is shown here to illustrate its form and content.

^a Air wavelengths are given for $\lambda > 2000$ Å and vacuum values below.

Table 3
Mean Abundances and Comparison with Previous Results

Spec.	N	$\log \epsilon$ (Ref. 1)	[X/Fe] (Ref. 1)	[X/Fe] (Ref. 2)	[X/Fe] (Ref. 3)
Mg I	1	4.23 (0.50)	+0.51 (0.45)	...	+0.51 (0.08)
Si I	10	3.78 (0.24)	+0.15 (0.22)	...	+0.54 (0.14)
P I	3	1.19 (0.28)	-0.34 (0.21)
S I	3	3.31 (0.45)	+0.07 (0.41)	...	< +1.11
Ti II	2	1.37 (0.28)	+0.30 (0.22)	+0.36 (0.20)	+0.41 (0.08)
Cr II	2	1.99 (0.23)	+0.23 (0.21)	-0.09 (0.21)	-0.17 (0.10)
Fe I	3	3.43 (0.28)	-4.07 (0.28)	-3.88 (0.19)	-3.83 (0.19)
Fe II	12	3.78 (0.24)	-3.72 (0.24)	-3.87 (0.17)	-3.82 (0.15)
Co II	4	1.76 (0.29)	+0.65 (0.23)	...	+0.59 (0.06) ^a
Ni I	3	2.26 (0.26)	-0.08 (0.21)	-0.02 (0.22)	+0.13 (0.06)
Ni II	3	2.27 (0.23)	-0.07 (0.21)	-0.13 (0.23)	...
Zn II	1	0.58 (0.32)	-0.10 (0.24)	...	< +0.22
As I	1	< -0.21	< +1.37
Se I	3	< -0.07	< +0.47

References. — 1: This study; 2: [Placco et al. \(2014a\)](#); 3: [Ito et al. \(2013\)](#)

Note. — All [X/Fe] ratios are computed using [Fe/H] = -3.88. [Fe/H] is listed for Fe I and Fe II.

^a [Co I/Fe]

desaturated by hyperfine splitting (HFS; [Lawler et al. 2015](#)). Laboratory data to reconstruct the HFS are not available at present, but the concordance between the [Co/Fe] ratios derived from Co I and Co II lines (Table 3) suggests we are not overestimating the Co abundance by neglecting Co II HFS (cf. [Snedden et al. 2016](#)).

Deviations from local thermodynamic equilibrium (i.e., non-LTE) are a persistent concern in abundance work. The Ti II, Cr II, and Zn II lines we use meet the “gold standard” criteria ([Lawler et al. 2013](#)): unsaturated lines arising from the ground and low-lying levels of the ion. These levels are the main population reservoirs of Fe-group atoms, and they should be well-characterized by LTE. The P I and S I lines we use arise from low-lying levels that comprise ~ 3 –55% of the neutral species, which are the dominant ionization states, so non-LTE overionization is expected to be minimal.

5. NEW ABUNDANCES IN BD+44°493

We have derived abundances from 10 Si I lines, whereas previously only a single optical Si I line had been detected in BD+44°493. We derive [Si/Fe] = $+0.15 \pm 0.22$. The statistical error in the Si abundance is only 0.06 dex; the error in [Si/Fe] is dominated by uncertainties in Fe and the model atmosphere parameters. Our derived [Si/Fe] ratio is lower than that derived previously ($+0.54 \pm 0.14$; [Ito et al. 2013](#)).

Our P abundance is 0.6 dex lower than the upper limit derived by [Roederer et al. \(2014c\)](#). The sub-solar [P/Fe] ratio in BD+44°493 (-0.34 ± 0.21) is also lower than the mean [P/Fe] ratio ($+0.04 \pm 0.10$) found by [Roederer et al.](#) for seven metal-poor carbon-normal stars. This could suggest a different origin for the P in BD+44°493, although a larger comparison sample is highly desirable.

Our S abundance is 0.9 dex lower than the upper limits derived by [Takeda & Takada-Hidai \(2011\)](#) and [Ito et al. \(2013\)](#). [S/Fe] exhibits the common α -enhanced plateau in other metal-poor stars ([S/Fe] $\approx +0.3$; [Nissen et al. 2007](#)), and the [S/Fe] ratio in BD+44°493 ($+0.07 \pm 0.41$) agrees with this value.

The [Zn/Fe] ratio (-0.10 ± 0.24) in BD+44°493 contrasts with other stars with [Fe/H] $\lesssim -3.3$, where

$+0.4 \lesssim [\text{Zn/Fe}] \lesssim +0.7$ (e.g., [Nissen et al. 2007](#)). Zn has been detected in one other CEMP-no star with [Fe/H] ~ -4 , CS 22949-037 ([Depagne et al. 2002](#)), where [Zn/Fe] is enhanced ($+0.7 \pm 0.1$). This suggests diverse conditions for Zn production in the progenitors of the CEMP-no stars.

We have also derived the first upper limits on the [As/Fe] and [Se/Fe] ratios for any CEMP star. These limits indicate that BD+44°493 is not enhanced in elements at the first r -process peak, similar to carbon-normal metal-poor stars ([Roederer 2012](#)).

6. DISCUSSION

The volatile elements C, N, O, S, and Zn are among the last to condense onto dust grains as a molecular cloud cools. [Venn & Lambert \(2008\)](#) proposed depletion of refractory elements on dust in a debris disk as an alternative explanation for the C enhancement and Fe-group depletions found in CEMP-no stars. While unlikely ([Venn et al. 2014](#)), this hypothesis predicts that [S/Fe] and [Zn/Fe] in BD+44°493 should be enhanced, similar to [C/Fe], [N/Fe], and [O/Fe]. The solar [S/Fe] and [Zn/Fe] ratios we have derived exclude this possibility. The [S/Fe] and [Zn/Fe] ratios could also result from a combination of dust depletion and low initial ratios produced by the progenitor SN ([Bonifacio et al. 2012](#)), but BD+44°493 presents evidence against this hypothesis as well. The mean condensation temperatures (T_C) of S and Zn are ~ 700 K ([Lodders 2003](#)), roughly half that of Si, Fe, and Ni ($T_C \sim 1350$ K). Si and S should share similar nucleosynthesis histories, as should Fe, Ni, and Zn. However, [X/H] ~ -3.9 for all five of these elements with different T_C , arguing against the dust-depletion hypothesis.

We assess the properties of the progenitor of BD+44°493 by comparing its abundance pattern with model predictions for Pop III SN yields. We use the 1D, non-rotating, single, massive star models from [Heger & Woosley \(2010\)](#). These models have masses 10–100 M_\odot , explosion energies $(0.3\text{--}10) \times 10^{51}$ erg, and vary the amount of mixing in the ejecta. We simulate 10^4 abundance patterns by resampling the observed ratios from normal distributions. We fit all abundances from C to Zn using a procedure similar to that described in [Placco et al. \(2015\)](#), using the `starfit` code⁵ to find the best model for each resampled pattern.

Figure 2 illustrates our results. The best-fit model, favored by 40% of the resampled abundance patterns, is a progenitor with initial mass 20.5 M_\odot , explosion energy 0.6×10^{51} erg, mixing factor $f_{\text{mix}} = 0.1$, ejected ^{56}Ni mass 0.0014 M_\odot , and remnant mass 5.47 M_\odot . More than 99% of the favored models have progenitor masses from 20.5–21.5 M_\odot and explosion energies from $(0.3\text{--}0.9) \times 10^{51}$ erg. Artificially inflating the uncertainties on [C/H], [N/H], and [O/H] to 0.4 dex broadens the range of masses and explosion energies, but $\sim 95\%$ of the beset-fit models encompass the same range as the standard case. BD+44°493 acquired about 0.001% of the metals ejected by this SN, and the low ($\ll 0.07 M_\odot$; [Nomoto et al. 2006](#)) ejected ^{56}Ni mass indicates that this is a faint SN.

The initial mass and explosion energy are somewhat lower than those favored previously (25 M_\odot , 5×10^{51} erg;

⁵ <http://starfit.org>

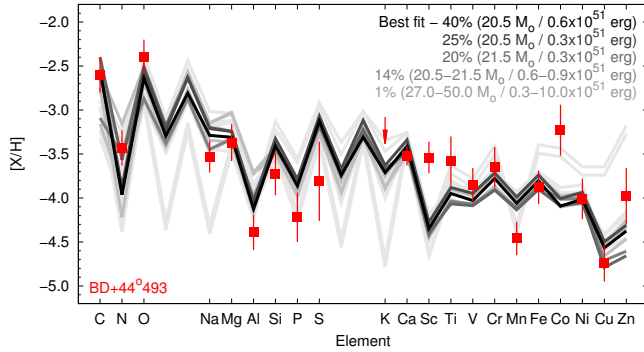


Figure 2. Best-fit models for the observed abundances of BD+44°493. The observational data are shown by red points. The masses and explosion energies of the models for the simulated abundance patterns are given in the upper right part of each panel, color-coded by the percentage of their occurrence.

Ito et al. 2013). This might be expected based on the lower $[\text{Zn}/\text{Fe}]$ ratio, which is sensitive to the explosion energy (e.g., Umeda & Nomoto 2005; Tominaga et al. 2007). These values are quite model dependent, and the range of acceptable values does not represent the true uncertainties. The enhanced $[\text{Co}/\text{Fe}]$ and solar $[\text{Zn}/\text{Fe}]$ cannot be fit simultaneously, but we note that model fits to CEMP-no stars often under-predict the $[\text{Co}/\text{Fe}]$ ratio (e.g., Tominaga et al. 2014). A higher progenitor mass and explosion energy with enhanced mixing may better explain the enhanced $[\text{Co}/\text{Zn}]$ ratio (cf. Nomoto et al. 2006), although this could exacerbate discrepancies with other elements (see discussion in Tominaga et al. 2014). Massive, rapidly-rotating, low-metallicity stars have also been proposed as the progenitors of CEMP-no stars like BD+44°493 (e.g., Maeder et al. 2015; Frischknecht et al. 2016), although no published grids of yields are yet available for comparison.

Our new observations of P, S, and Zn in BD+44°493 demonstrate that COS can be used for abundance work in late-type stars. This may enable new theoretical comparisons and motivate observational campaigns to study these elements in the earliest generations of stars.

Generous support for Program GO-14231 has been provided by a grant from STScI, which is operated by AURA, under NASA contract NAS5-26555. Partial support has also been provided by grant PHY 14-30152 (Physics Frontier Center/JINA-CEE) awarded by the U.S. National Science Foundation (NSF). We thank J. Lawler and N. Tominaga for helpful discussions. We also thank the referee for many helpful suggestions. This research has made use of NASA’s Astrophysics Data System Bibliographic Services; the arXiv pre-print server operated by Cornell University; the SIMBAD and VizieR database hosted by the Strasbourg Astronomical Data Center; the Atomic Spectra Database hosted by the National Institute of Standards and Technology; the MAST at STScI; IRAF software packages distributed by the National Optical Astronomy Observatories, which are operated by AURA, under cooperative agreement with the NSF; and the R software package (R Core Team 2014).

Facilities: HST (COS)

REFERENCES

- Aoki, W. 2015, *ApJ*, 811, 64
- Asplund, M., Grevesse, N., Sauval, A. J., & Scott, P. 2009, *ARA&A*, 47, 481
- Beers, T. C., & Christlieb, N. 2005, *ARA&A*, 43, 531
- Bergeson, S. D., & Lawler, J. E. 1993, *ApJ*, 408, 382
- Bonifacio, P., Caffau, E., Venn, K. A., & Lambert, D. L. 2012, *A&A*, 544, A102
- Carney, B. W., Latham, D. W., Stefanik, R. P., Laird, J. B., & Morse, J. A. 2003, *AJ*, 125, 293
- Carollo, D., Beers, T. C., Bovy, J., et al. 2012, *ApJ*, 744, 195
- Castelli, F., & Kurucz, R. L. *Proc. IAU Symp. No 210, Modelling of Stellar Atmospheres*, N. Piskunov et al., eds. 2003, A20
- Cooke, R., Pettini, M., Steidel, C. C., Rudie, G. C., & Jorgenson, R. A. 2011, *MNRAS*, 412, 1047
- Depagne, E., Hill, V., Spite, M., et al. 2002, *A&A*, 390, 187
- Fedchak, J. A., & Lawler, J. E. 1999, *ApJ*, 523, 734
- Frebel, A., Simon, J. D., Geha, M., & Willman, B. 2010, *ApJ*, 708, 560
- Frischknecht, U., Hirschi, R., Pignatari, M., et al. 2016, *MNRAS*, 456, 1803
- Ghavamian, P., Aloisi, A., Lennon, D., et al. 2009, COS Instrument Science Report 2009-01(v1) (Baltimore, MD: STScI)
- Green, J. C., Froning, C. S., Osterman, S., et al. 2012, *ApJ*, 744, 60
- Hansen, T. T., Andersen, J., Nordström, B., et al. 2016, *A&A*, 586, A160
- Heger, A., & Woosley, S. E. 2010, *ApJ*, 724, 341
- Ishigaki, M. N., Tominaga, N., Kobayashi, C., & Nomoto, K. 2014, *ApJ*, 792, L32
- Ito, H., Aoki, W., Honda, S., & Beers, T. C. 2009, *ApJ*, 698, L37
- Ito, H., Aoki, W., Beers, T. C., Tominaga, N., et al. 2013, *ApJ*, 773, 33
- Lawler, J. E., Guzman, A., Wood, M. P., Sneden, C., & Cowan, J. J. 2013, *ApJS*, 205, 11
- Lawler, J. E., Sneden, C., & Cowan, J. J. 2015, *ApJS*, 220, 13
- Lodders, K. 2003, *ApJ*, 591, 1220
- Maeder, A., Meynet, G., & Chiappini, C. 2015, *A&A*, 576, A56
- Meynet, G., Ekström, S., & Maeder, A. 2006, *A&A*, 447, 623
- Nilsson, H., Ljung, G., Lundberg, H., & Nielsen, K. E. 2006, *A&A*, 445, 1165
- Nissen, P. E., Akerman, C., Asplund, M., et al. 2007, *A&A*, 469, 319
- Nomoto, K., Tominaga, N., Umeda, H., Kobayashi, C., & Maeda, K. 2006, *Nuclear Physics A*, 777, 424
- Norris, J. E., Yong, D., Bessell, M. S., et al. 2013, *ApJ*, 762, 28
- Placco, V. M., Beers, T. C., Roederer, I. U., et al. 2014a, *ApJ*, 790, 34
- Placco, V. M., Frebel, A., Beers, T. C., & Stancliffe, R. J. 2014b, *ApJ*, 797, 21
- Placco, V. M., Frebel, A., Lee, Y. S., et al. 2015, *ApJ*, 809, 136
- R Core Team. 2014. “R: A language and environment for statistical computing,” R Foundation for Statistical Computing, Vienna, Austria. URL <http://www.R-project.org/>.
- Roederer, I. U. 2012, *ApJ*, 756, 36
- Roederer, I. U., & Lawler, J. E. 2012, *ApJ*, 750, 76
- Roederer, I. U., Preston, G. W., Thompson, I. B., Shectman, S. A., & Sneden, C. 2014a, *ApJ*, 784, 158
- Roederer, I. U., Preston, G. W., Thompson, I. B., et al. 2014b, *AJ*, 147, 136
- Roederer, I. U., Jacobson, H. R., Thanathibodee, T., Frebel, A., & Toller, E. 2014c, *ApJ*, 797, 69
- Sneden, C. A. 1973, Ph.D. Thesis, Univ. of Texas at Austin
- Sneden, C., Cowan, J. J., Kobayashi, C., et al. 2016, *ApJ*, 817, 53
- Sobeck, J. S., Kraft, R. P., Sneden, C., et al. 2011, *AJ*, 141, 175
- Takeda, Y., & Takada-Hidai, M. 2011, *PASJ*, 63, 537
- Takeda, Y., & Takada-Hidai, M. 2013, *PASJ*, 65, 65
- Tominaga, N., Umeda, H., & Nomoto, K. 2007, *ApJ*, 660, 516
- Tominaga, N., Iwamoto, N., & Nomoto, K. 2014, *ApJ*, 785, 98
- Umeda, H., & Nomoto, K. 2003, *Nature*, 422, 871
- Umeda, H., & Nomoto, K. 2005, *ApJ*, 619, 427
- Venn, K. A., & Lambert, D. L. 2008, *ApJ*, 677, 572
- Venn, K. A., Puzia, T. H., Divell, M., et al. 2014, *ApJ*, 791, 98
- Wood, M. P., Lawler, J. E., Sneden, C., & Cowan, J. J. 2014, *ApJS*, 211, 20